

Quantum Spin Hall Effect in Two-dimensional Crystals of Transition Metal Dichalcogenides

M. A. Cazalilla,^{1,2} H. Ochoa,³ and F. Guinea³

¹*Department of Physics, National Tsing Hua University,
and National Center for Theoretical Sciences (NCTS), Hsinchu City, Taiwan.*

²*Donostia International Physics Center (DIPC),
Manuel de Lardizabal 4, 20018, San Sebastian, Spain.*

³*Instituto de Ciencia de Materiales de Madrid (ICMM). CSIC, Cantoblanco. E-28049 Madrid. Spain.*

(Dated: September 4, 2018)

We propose to engineer time-reversal-invariant topological insulators in two-dimensional (2D) crystals of transition metal dichalcogenides (TMDCs). We note that, at low doping, semiconducting TMDCs under shear strain will develop spin-polarized Landau levels residing in different valleys. We argue that gaps between Landau levels in the range of 10–100 Kelvin are within experimental reach. In addition, we point out that a superlattice arising from a Moiré pattern can lead to topologically non-trivial subbands. As a result, the edge transport becomes quantized, which can be probed in multi-terminal devices made using strained 2D crystals and/or heterostructures. The strong d character of valence and conduction bands may also allow for the investigation of the effects of electron correlations on the topological phases.

PACS numbers: 85.75.-d, 73.43.Qt, 73.43.-f

There is currently much interest in two-dimensional (2D) crystals of transition metal dichalcogenides (TMDC) such as MoS₂ or WSe₂ [1]. Compared to Graphene, many of these materials are semiconductors with sizeable gaps (≈ 1 eV), which makes them good candidates for applications in conventional electronics such as the manufacture of transistors [2].

By contrast, the quantum spin Hall (QSH) effect [3] has been postulated as the paradigm for future *non-dissipative* nano-electronics [4]. Indeed, provided that magnetic impurities (or other time-reversal symmetry-breaking perturbations) can be eliminated, electron transport through the edge of a QSH insulator becomes ballistic. This is because counter propagating channels of the same spin are spatially separated.

Nevertheless, the QSH effect has been observed in very few materials [5, 6] so far, making the search for new systems exhibiting this effect a major scientific endeavor. In the context of 2D crystals, Weeks and coworkers have recently proposed an approach to enhance the spin-orbit coupling in graphene by heavy ad-atom deposition [7], which could lead to a realization of the Kane-Mele model [8] and the QSH effect. The availability of 2D materials exhibiting this effect may allow for the construction of flexible electronic devices with low-power consumption.

In this work, we present a proposal for engineering the QSHE in strained 2D crystals and heterostructures made using TMDCs. Strain is known to induce pseudo-magnetic fields in 2D crystals [9–11]. These fields have been predicted [9] and experimentally found [10] to produce Landau levels (LLs) in the electronic spectrum of 2D crystals such as graphene. As explained below, it is also possible to exploit these pseudo-magnetic fields

to engineer time-reversal invariant topological phases in other 2D crystals such as the TMDCs. This approach has several attractive features. Using MoS₂ as an example, we find that gaps between LLs scale as $\hbar\omega_c/k_B \simeq 2.7 B_0[T]$ K, where $B_0[T]$ is the strength of the pseudo-magnetic field in Tesla. Fields $B_0[T] \sim 10 - 10^2$ T have been experimentally demonstrated [9, 10], which in the case of TMDCs could lead to LL gaps of up to ≈ 100 K. By comparison, the gaps achievable by straining GaAs are in the range of tens of milli-Kelvin [12]. The much larger magnitude of the LLs gaps in the present proposal stems the strain coupling to the electron current, rather than the electron spin current as in Ref. [12]. These two coupling constants are, in general, vastly different in order of magnitude. However, in multi-valley systems like graphene, strain only leads to (spin) unpolarized LLs. What sets semiconducting TMDCs apart is the spin-orbit coupling (SOC) that produces a large spin splitting of the valence (and to a smaller extent, the conduction) band. For small doping, this leads to spin-polarized LLs in different valleys, which opens the possibility of realizing time-reversal invariant (TRI) topological phases. Furthermore, the valence and conduction band of semiconducting TMDC have strong d character [13], which, along with the poor screening of the Coulomb interaction in 2D, means that electron interactions can have interesting effects on properties of the TRI topological phases realized in TMDCs.

Bulk TMDC are composed of X - M - X layers stacked on top of each other and coupled by weak Van der Waals forces. Therefore, like graphite, these materials can be exfoliated down to a single layer. The transition metal atoms (M) are arranged in a triangular lattice and each one is bonded to six chalcogen atoms (X) (see Fig. 1 for

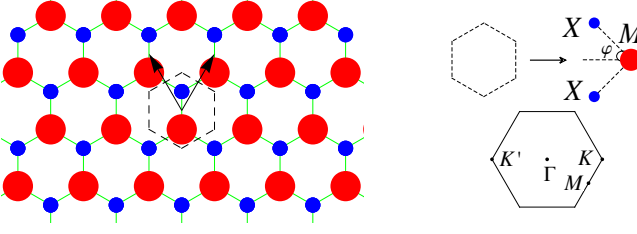


FIG. 1: (Color Online) Top view of the 2D lattice of TMDC. The unit cell and Brillouin zone are shown in the right panel. M corresponds to the transition metal atom, whereas X to the chalcogen atoms.

a top view of the lattice). The point group of the 2D crystal is D_{3h} . The Fermi level lies at the two inequivalent corners of the Brillouin zone, K and K' points, as in the case of graphene, but the spectrum is gapped. The character of the conduction and valence bands is dominated by $d_{3z^2-r^2}$ and $d_{x^2-y^2} \pm id_{xy}$ orbitals from M atom, respectively, where the sign $+$ ($-$) holds for K (K') point. Furthermore, both bands have a non-negligible hybridization with the bonding combination of $p_x \pm ip_y$ (in the conduction band) and $p_x \mp ip_y$ (in the valence band) orbitals from X atoms.

In the continuum limit, the system is well described by the following two-band Hamiltonian [2, 13, 15]:

$$H_0 = v(\tau^z \sigma^x p_x + \sigma^y p_y) + \Delta \sigma^z + \frac{\lambda_{\text{SO}}}{2} \tau^z s^z (1 - \sigma^z), \quad (1)$$

where $\mathbf{p} = (p_x, p_y)$ is the electron crystal momentum referred to the K (K') point, for which we introduce $\tau^z = +1$ ($\tau^z = -1$); σ^α are Pauli matrices acting on the space span by conduction and valence band states; Δ is the band gap and $v = ta/\hbar$, where a is the lattice parameter and t is a phenomenological hybridization parameter; finally, s^z is the spin projection along the z axis perpendicular to the 2D crystal. The Hamiltonian (1) can be constructed phenomenologically by considering scalar invariants of D_{3h} formed from operators σ^α , \mathbf{p} and spin s^α . The symmetry properties of these operators are listed in Table I. Besides the gap, another important difference with graphene is the spin splitting of the bands due to the strong spin-orbit interaction provided by M atoms. Below, we focus on p-doped TMDCs, which allows us to neglect the smaller spin splitting of the conduction band [15]. For the valence band, the latter is in the range of 100-400 meV depending on the material [16, 18, 19]. The Hamiltonian (1) can be also derived from a microscopic theory. From a simplified tight-binding model [17], we obtain $\Delta = 1.41$ eV and $t = 1.19$ eV.

In order to turn a TMDC into a TRI topological insulator, we need to consider the effect of strain on the band structure. Strain is described by a rank-2 tensor, $u_{\alpha\beta} = \frac{1}{2}(\partial_\alpha u_\beta + \partial_\beta u_\alpha + \frac{\partial h}{\partial x_\alpha} \frac{\partial h}{\partial x_\beta})$, where $\mathbf{u} = (u_x, u_y)$ (h) is the in-plane (out-of-plane) displacement of the unit cell

Irrep	TR Even	TR Odd
A'_1	$1, \sigma^z, \sum_\alpha u_{\alpha\alpha}$	-
A'_2	-	τ^z, s^z
E'	$(\sigma^x, \tau^z \sigma^y), (u_{xx} - u_{yy}, -2u_{xy})$	$(\tau^z \sigma^x, \sigma^y), \mathbf{p} = (p_x, p_y)$
E''	-	(s^x, s^y)

TABLE I: Symmetry classification of the electronic operators and strain tensor components according to the irreducible representations (Irrep) of D_{3h} and time reversal operation.

in the long-wave length limit. The three components of $u_{\alpha\beta}$ can be split according to irreducible representations of D_{3h} as shown in Table I. Thus, the coupling with strain reads:

$$H_{\text{strain}} = \beta_0 t \sum_\alpha u_{\alpha\alpha} + \beta_1 t \sum_\alpha u_{\alpha\alpha} \sigma^z + \beta_2 t [(u_{xx} - u_{yy}) \sigma^x - 2u_{xy} \tau^z \sigma^y]. \quad (2)$$

Microscopically, the origin of these couplings is the change in the hybridization between d orbitals from M atoms and p orbitals from X atoms due to the distortion of the lattice. In our microscopic tight-binding model [17], the phenomenological constants $\beta_{0,1,2}$ are given by the Grüneisen parameters [11] associated to the hopping amplitudes considered in the calculation [17]. The trace of the strain tensor generates scalar potentials of different strength in the valence and conduction bands. In addition, strain can be introduced in Eq. (1) as a minimal coupling $\mathbf{p} \rightarrow \mathbf{p} - e\mathbf{A}$ to a vector potential $e\mathbf{A} = \frac{\hbar\beta_2}{a} \tau^z (u_{yy} - u_{xx}, 2u_{xy})$. The presence of τ^z indicates that the pseudo-magnetic field has opposite sign on different valleys, which is necessary as strain does not violate TRI.

Henceforth, we assume that the system is doped with holes and therefore the Fermi level crosses the valence band. Integrating out the conduction band to leading order in Δ^{-1} yields:

$$H_v = -\frac{\Pi_+(\tau^z)\Pi_-(\tau^z)}{2m^*} + U(\mathbf{r}) + \lambda_{\text{SO}} s^z \tau^z, \quad (3)$$

where $m^* = \Delta/2v^2 \simeq 0.5$ [22], $U(\mathbf{r}) = g(u_{xx} + u_{yy})$ with $g = t(\beta_0 - \beta_1)$, and $\Pi_\pm(\tau^z) = (\tau^z p^x \pm ip^y) - e(\tau^z A_x \pm iA_y)$, which obey the commutation relation $[\Pi_+(\tau^z), \Pi_-(\tau^z)] = 2e\hbar\tau^z B(\mathbf{r})$, where $B(\mathbf{r}) = \partial_x A_y - \partial_y A_x$. Corrections of $\mathcal{O}(\Delta^{-2})$ have been also obtained and can lead to mixing of the Landau levels, but they can be neglected as for typical parameters $\hbar\omega_c \lesssim 10^{-2}\Delta$.

In the absence of strain (i.e. $\mathbf{A} = U = 0$), Eq. (3) describes the Bloch states at the top of the valence band near K, K' . Owing to the spin-orbit coupling ($\propto \lambda_{\text{SO}}$), for small hole doping (i.e. $|\epsilon_F| \ll \lambda_{\text{SO}}$), the spin and valley spin of the holes are locked to each other, i.e. only holes with either (K, \uparrow) or (K', \downarrow) can exist (cf. Fig. 2). Furthermore, the states at K and K' are Kramers pairs.

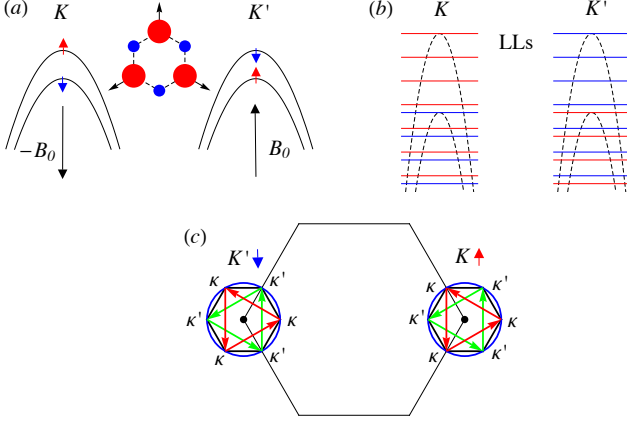


FIG. 2: (Color Online) (a) Low-energy spectrum of a semiconducting transition metal dicalchogenide around the K and K' points of the first Brillouin zone described by the continuum-limit Hamiltonian in Eq. (3). The inset shows the orientation of the stress tensor field discussed through the text with respect to the lattice. (b) Schematic representation of the Landau Levels (LLs) induced in the valence band when strain is applied. (c) A superlattice can be also used to create a topologically non-trivial subband structure. A triangular superlattice produces replicas of K and K' by mixing the valence and conduction band states at the mini-Dirac points as indicated by the arrows.

This feature is crucial for the realization of a time-reversal invariant topological phase, as we argue below.

Applying a pure shear strain, i.e. $u_{xx} + u_{yy} = 0$ (i.e. $U = 0$), and $u_{xx} = -u_{yy} = -C\gamma$, $u_{xy} = -Cx$, we have $B_z(\mathbf{r}) = \partial_x A_y - \partial_y A_x = -\tau^z B_0$ with $B_0 = \frac{4C\hbar\beta_2}{ea} > 0$ [20]. The Hamiltonian in (3) can be diagonalized after introducing $a_K = \Pi_-(\tau^z = +1)/\sqrt{2e\hbar B_0}$ and $a_{K'} = \Pi_-(\tau^z = -1)/\sqrt{2e\hbar B_0}$:

$$H = -\hbar\omega_c \left(a_K^\dagger a_K + a_{K'}^\dagger a_{K'} \right) + \lambda_{\text{SO}} s^z \tau^z, \quad (4)$$

where $\omega_c = eB_0/m^*$. As stated above, even for the largest achievable pseudo-magnetic fields ($B_0 \sim 10^2$ T) $\hbar\omega_c \ll \lambda_{\text{SO}}$, and therefore, provided $|\epsilon_F| \ll \lambda_{\text{SO}}$, LLs at different valleys are occupied by holes with opposite spin. The resulting model has been shown by Bernevig and Zhang [12] to display the QSH effect, meaning that the Hall conductivity σ_H^{xy} is zero but the spin-Hall conductivity σ_{sH}^{xy} is quantized in units of $2e/4\pi$.

The strain configuration described above can be created by the methods described in Ref. [9]. For a TMDC 2D crystal flake under trigonal strain [9] (cf. Fig. 2), one concern is the sample size. The latter is limited by the maximum tensile strength of the TMDCs, T_{max} . For MoS₂, the thermodynamic relation $\sigma_{\alpha\beta} = 2\mu u_{\alpha\beta}$ ($\sigma_{\alpha\beta}$ being the stress tensor and μ is the shear modulus) allows us to estimate the maximum sample size $L \approx \frac{2T_{\text{max}}}{\mu C}$. The values of $\mu \simeq 50.4$ N/m and $T_{\text{max}} \simeq 16.5$ N/m can be obtained from density-functional calculations [21].

This yields a relation between the maximum pseudo-magnetic field (in Tesla) and the sample size L in μm : $B_0[\text{T}] \approx 8/L[\mu\text{m}]$. Using $\hbar\omega_c/k_B = 2.7 B_0[\text{T}]$ and taking $L \approx 1 \mu\text{m}$, we estimate $\hbar\omega_c/k_B \simeq 20$ K for MoS₂.

For small strained 2D crystal flakes, it is necessary to take into account the effect of an inhomogeneous pseudo-magnetic field resulting from a non-uniform strain distribution. In this regard, we note that the lowest LL eigenfunctions are null eigenvectors of $\Pi_-(\tau^z)$:

$$\Pi_-(\tau^z)\psi(\mathbf{r}) = 0, \quad (5)$$

Therefore, following [32], we write $\mathbf{A}(\mathbf{r}) = \tau_z(\hat{\mathbf{z}} \times \nabla\chi(\mathbf{r}) + \nabla\phi(\mathbf{r}))$, which allows to solve (5) for K [K'] and yields $\psi(\mathbf{r}) = f(z^*)e^{\frac{2\pi}{\Phi_0}(\chi(\mathbf{r}) + i\phi(\mathbf{r}))}$ [$\psi(\mathbf{r}) = f(z)e^{\frac{2\pi}{\Phi_0}(\chi(\mathbf{r}) - i\phi(\mathbf{r}))}$], where $f(z^*)$ [$f(z)$] is a polynomial of $z = (x + iy)$ [$z^* = (x - iy)$] of maximum degree $N = [\Phi/\Phi_0]$, $\Phi = \int d\mathbf{r} B_0(\mathbf{r}) > 0$ being the total flux and $\Phi_0 = h/e$ the flux quantum [33]. Hence, the wave-function describing $N_\uparrow = N_\downarrow = N$ (non-interacting) electrons in the lowest LL reads [32]:

$$\Phi_0(\{\mathbf{r}_{i\alpha}\}) = e^{-F} \prod_{i < j} (z_{i\uparrow}^* - z_{j\uparrow}^*)(z_{i\downarrow} - z_{j\downarrow}), \quad (6)$$

where $F(\{\mathbf{r}_{i\alpha}\}) = \frac{2\pi}{\Phi_0} \sum_{i=1, \alpha=\uparrow, \downarrow}^N [\chi(\mathbf{r}_{i\alpha}) - i\alpha\phi(\mathbf{r}_{i\alpha})]$.

Larger sample sizes can be achieved by other methods such in 2D crystal bubbles [9, 10]. A periodic array of such bubbles will lead to periodic modulation of strain and pseudo-magnetic field, which allows to create topologically non-trivial band structures [9, 23]. Alternatively, a superlattice can be used to create, within each valley, a band with non trivial topological properties. If we neglect trigonal warping, each valley has a time-reversal-like symmetry where $\Psi_{A/B}(\vec{\mathbf{r}}) \rightarrow \Psi_{A/B}^*(\vec{\mathbf{r}})$. This symmetry is broken by "gauge" terms proportional to σ_x and σ_y in Eq. (1), which can arise from strain or from virtual hopping processes to the substrate [17]. A suitable combination of periodic scalar and a gauge potentials can [24]: i) separate the lowest leading subbands from the rest by opening a gap at the edges of the superlattice Brillouin Zone (see Fig. 2), and ii) give a total Chern number of ± 1 to the subbands arising at the K, K' valleys, respectively. This approach, which relies on a periodic magnetic field with zero average leads to a Quantum Hall insulator [25] in the absence of a global magnetic flux [26]. The periodicity of the potential should be such that the width of the subbands is smaller than the spin splitting in each valley. Large enough periodicities where subbands can be resolved have been achieved for graphene on Boron Nitride [27–30]. A different scheme leading to the QSH effect based on a Moiré pattern in a single valley semiconductor like GaAs is suggested in [31].

We next discuss some experimental consequences of our predictions. As mentioned above, the Hall conductivity σ_H^{xy} is zero but the spin-Hall conductivity σ_{sH}^{xy} is

quantized in units of $2e/4\pi$ [12]. However, if the total s^z is not a good quantum number (see discussion below), σ_{sH}^{xy} is not exactly quantized [3]. Instead, charge transport through the (helical) edge channels provides a clearer signature of existence of a topological phase [5, 6].

Nevertheless, in the case of strained crystals in the absence of a superlattice potential, we must be careful in qualifying the strained 2D crystal as a topological insulator for arbitrary LL filling. This is because adatoms, a perpendicular electric field, out of plane deformations, etc. break the mirror symmetry about the 2D crystal plane, which induces a Rashba spin-orbit coupling $\sim (\tau^z \sigma^x s^y - \sigma^y s^x)$ in the Hamiltonian of Eq. (1). Rashba allows for spin flips and therefore can lead to backscattering between counter-propagating edge channels. For an odd number of occupied LLs, an odd number of Kramers' pairs of edge modes cross the Fermi energy and, for weak to moderate electron-electron interactions, the integrity of at least one Kramers' pair of edge modes against TRI perturbations that induce spin-flip scattering like Rashba spin-orbit coupling is always ensured [34]. Thus, for $2n+1$ (with n integer) occupied LLs, the system is TRI protected topological phase and a two-terminal measurement of the conductance will yield at least $2e^2/h$ and at most $2(2n+1)e^2/h$, depending of degree of edge disorder and other s^z non-conserving perturbations.

On the other hand, if the number of occupied LLs is even ($= 2n$), there will an even number of pairs of edge modes crossing the Fermi level and this situation is no longer protected against e.g. Rashba-type disorder potential [34] (although edge modes survive for strong enough electron-electron interactions [34]). However, in sufficiently clean samples and provided interactions are weak, quantized conductance of $4ne^2/h$ may be observable. Furthermore, the existence of bulk LLs can be detected by means of scanning tunneling microscopy as in the case of graphene [10].

Finally, let us discuss the possible effect of interactions. The strong d character of the valence and conduction bands means that electron correlations can have a important effect on the topological phases, especially on the edge states [34, 36]. Indeed, for MoS_2 the short-range part of the interaction (i.e. the Hubbard- U) has been estimated in Ref. [35] to be ~ 2 -10 eV. Thus, MoS_2 may present a scenario comparable to the Iridates [36]. However, the QSH effect in the TMDCs may allow for a more complete understanding of the interplay between electron correlation and QSH physics, since correlation effects decrease as the metal atom M is varied from the $4d$ series (as in MoS_2) to $5d$ series (as in WS_2).

In conclusion, we have presented a proposal to engineer time-reversal invariant topological phases in 2D crystals of transition metal dicalchogenides (TMDC) under strain and/or in heterostructures which induce superlattice potentials. We also note that the proposal can be extended to electron-doped TMDC. However,

in this case, the separation between the Landau levels ($\hbar\omega_c/k_B \simeq 2.2 B_0[T]$) and the strength of the superlattice potential are limited by the much smaller spin-orbit coupling ($\lambda_{\text{SO}} \sim 10 \text{ meV} \sim 100 \text{ K}$) [16], which also requires much lower temperatures. We hope that the feasibility of our proposal will stimulate further experimental work along these directions. We stress that compared to other QSH systems [5, 6], strained 2D TMDCs allow for much larger tunability of material parameters as well as the strength of the Berry curvature responsible for the Landau levels. In this regard, the main obstacle for the observation of the QSH effect appears to be the reduced carrier mobility in currently available 2D crystals of TMDCs. However, given the notorious technological potential of these materials, we expect this obstacle will be overcome in the near future.

MAC acknowledges financial support from a start-up fund from NTHU and NCS and NCTS (Taiwan). HO acknowledges financial support through a JAE-Pre grant (CSIC, Spain). FG acknowledges support from the Spanish Ministry of Economy (MINECO) through Grant no. FIS2011-23713, the European Research Council Advanced Grant (contract 290846) and from European Commission under the Graphene Flagship contract CNECT-ICT-604391.

-
- [1] Q. H. Wang, K. Kalantar-Zadeh, A. Kiss, J. N. Coleman, and M. S. Strano, *Nature Nanotech* **7**, 699 (2012) and references therein.
 - [2] B. Radisavljevic, A. Radenovic, J. Brivio, V. Giacometti, and A. Kis, *Nature Nanotechnology*, **6**, 147 (2011); H. Nam, S. Wi, H. Rokni, M. Chen, G. Priessnitz, W. Lu, and X. Liang, *ACS Nano*, **7**, 5870 (2013).
 - [3] M. Z. Hassan and C. L. Kane, *Rev. Mod. Phys.* **82**, 3045 (2010); X.-L. Qi and S.-C. Zhang, *ibid* **83**, 1057 (2011); B. A. Bernevig with T. L. Hughes, *Topological Insulators and Topological Superconductors*, Princeton Univ. Press, (Princeton 2013), and references therein.
 - [4] See e.g. talk by S.-C. Zhang, available from http://www.aip.org/industry/ipf/2011/day2_8_Zhang/
 - [5] M. König, S. Wiedmann, C. Brüne, A. Roth, H. Buhmann, L. W. Molenkamp, X.-L. Qi, S.C. Zhang, *Science* **308**, 766 (2007).
 - [6] I. Knez, R.-R. Du, G. Sullivan, *Phys. Rev. Lett.* **107**, 136603 (2011)
 - [7] C. Weeks, J. Hu, J. Alicea, M. Franz, and R. Wu, *Physical Review X* **1**, 021001 (2011).
 - [8] C. L. Kane and E. J. Mele, *Phys. Rev.* **95**, 226801 (2013).
 - [9] F. Guinea, M. I. Katsnelson, and A. K. Geim, *Nature Physics*, **6**, 30 (2010).
 - [10] N. Levy *et al.* *Science* **329**, 544 (2010); J. Lu, A.H. Castro Neto, and K. P. Loh, *Nature Comm.* **3**, 823 (2011).
 - [11] M. A. Vozmediano, M. I. Katsnelson, and F. Guinea, *Physics Reports* **496**, 109 (2010).
 - [12] B. A. Bernevig and S.-C. Zhang, *Phys. Rev. Lett.* **96**, 106802 (2006).
 - [13] D. Xiao, G.-B. Liu, W. Feng, X. Xu, and W. Yao, *Phys.*

- Rev. Lett. **108**, 196802 (2012). **88**, 045416 (2013).
- [14] E. Cappelluti, R. Roldán, J.A. Silva-Guilln, P. Ordejón, F. Guinea, Phys. Rev. B **88**, 075409 (2013).
- [15] H. Ochoa and R. Roldán, Phys. Rev. B **87**, 245421 (2013).
- [16] Z. Y. Zhu, Y. C. Cheng, and U. Schwingenschlögl, Phys. Rev. B **84**, 153402 (2011); W. Feng, Y. Yao, W. Zhu, J. Zhou, W. Yao, and D. Xiao, *ibid* **86**, 165108 (2012); A. Kormányos, V. Zólyomi, N. D. Drummond, P. Rakya, G. Burkard, V. I. Fal'ko, *ibid* **88**, 045416 (2013).
- [17] See supplementary material.
- [18] W. Jin *et al.* Phys. Rev. Lett. **111**, 106801 (2013); S. K. Mahatha, K. D. Patel, and K. S. R. Menon, J. Phys. Cond. Matt. **24** 475504 (2012).
- [19] K. F. Mak *et al.* Phys. Rev. Lett. **105**, 136805 (2010); W. S. Yun *et al.* Phys. Rev. B **85**, 033305 (2012).
- [20] We take $C > 0$ and assume $\beta \approx 3$ according to M. Buscema *et al.* ACS Nano Lett. **13**, 358 (2013).
- [21] R. C. Cooper, C. Lee, C. A. Marianetti, X. Wei, J. Hone, and J. W. Kysar, Phys. Rev. B **87**, 035423 (2013). The value of μ is obtained from the calculated Young's modulus E and Poisson's ratio ν as $\mu = \frac{E}{2(1+\nu)}$.
- [22] This is the effective mass inferred from the tight-binding model. The actual hole effective mass is slightly anisotropic [16]. We take $m^* = 0.5$ and neglect the anisotropy.
- [23] M. Taillefumier *et al.* Phys. Rev. B **78**, 155330 (2008).
- [24] T. Low, F. Guinea, and K. I. Katsnelson, Phys. Rev. B **83** 195436 (2011).
- [25] I. Snyman, Phys. Rev. B **80**, 054303 (2009).
- [26] F. D. M. Haldane, Phys. Rev. Lett. **61**, 2015 (1988).
- [27] M. Yankowitz *et al.*, Nature Phys. **8**, 382 (2012).
- [28] L. A. Ponomarenko *et al.*, Nature **497**, 594 (2013).
- [29] C. R. Dean *et al.*, Nature **497**, 598 (2013).
- [30] B. Hunt *et al.*, Science **340**, 1427 (2013).
- [31] O. P. Sushkov, and A. H. Castro Neto, Phys. Rev. Lett. **110**, 186601 (2013).
- [32] Y. Aharonov and A. Casher, Phys. Rev. A **19**, 2461 (1979); M. Bander, Phys. Rev. B **41**, 9028 (1990).
- [33] Φ is assumed to be positive as in the uniform case. Note that $\chi(\mathbf{r}) = -\int \frac{d\mathbf{r}'}{2\pi} \ln(|\mathbf{r} - \mathbf{r}'|) B_0(\mathbf{r}') \sim -\frac{\Phi}{2\pi} \ln(|\mathbf{r}|)$ as $|\mathbf{r}| \rightarrow \infty$, and therefore $\psi(\mathbf{r}) \sim f(x + i\tau_z y) |\mathbf{r}|^{-\frac{\Phi}{\Phi_0}}$.
- [34] C. Xu and J. Moore, Phys. Rev. B **73** 045322. (2006); C. Wu, B. A. Bernevig, and S.-C. Zhang, Phys. Rev. Lett. **96**, 106401 (2006).
- [35] R. Roldán, E. Cappelluti, and F. Guinea, Phys. Rev. B **88**, 054515 (2013).
- [36] A. Shitade *et al.*, Phys. Rev. Lett. **102**, 256403 (2009)

SUPPLEMENTARY INFORMATION

Microscopic derivation of the two-bands Hamiltonian

Tight-binding model

We consider a simplified tight-binding Hamiltonian acting on the subspace span by the symmetry-adapted Bloch wave functions $|\text{M } d_{3z^2-r^2}\rangle$, $|\text{M } d_{x^2-y^2} + \tau i d_{xy}\rangle$, $|\text{X (b) } p_y + i\tau p_x\rangle$, and $|\text{X (b) } p_y - i\tau p_x\rangle$. The model is strictly valid around \mathbf{K}_τ points, where $\tau = \pm 1$ labels the two valleys K ($\tau = +1$) and K' ($\tau = -1$). The crystal field parameters are:

$$\begin{aligned} \langle \text{M } d_{3z^2-r^2} | \mathcal{H}_{TB} | \text{M } d_{3z^2-r^2} \rangle &= \Delta_0 \\ \langle \text{M } d_{x^2-y^2} + \tau i d_{xy} | \mathcal{H}_{TB} | \text{M } d_{x^2-y^2} + \tau i d_{xy} \rangle &= \Delta_2 \\ \langle \text{X (b) } p_y \pm \tau i p_x | \mathcal{H}_{TB} | \text{X (b) } p_y \pm \tau i p_x \rangle &= \Delta_p. \end{aligned} \quad (7)$$

The hopping integrals sketched in Fig. 3 can be expressed in terms of the two-center Slater-Koster parameters $V_{dp\sigma}$, $V_{dp\pi}$ [1] as follows:

$$\begin{aligned} t_x &= \frac{\sqrt{3}}{2} V_{pd\sigma} \cos \varphi \\ t_y &= -V_{pd\pi} \cos \varphi \\ t_z &= \cos \varphi \left(\sin^2 \varphi - \frac{1}{2} \cos^2 \varphi \right) V_{pd\sigma} - \sqrt{3} \cos \varphi \sin^2 \varphi V_{pd\pi}, \end{aligned} \quad (8)$$

where the angle φ is defined in the main text. The matrix elements between Bloch states of orbitals of M and X atoms at \vec{q} read:

$$\begin{aligned} \langle \text{M } d_{3z^2-r^2} | \mathcal{H}_{TB} | \text{X (b) } p_y \pm i\tau p_x \rangle &= \sum_{\hat{\delta}} e^{-ia\vec{q} \cdot \hat{\delta}} t_z (\hat{y} \pm i\tau \hat{x}) \cdot \hat{\delta} \\ \langle \text{M } d_{x^2-y^2} + \tau i d_{xy} | \mathcal{H}_{TB} | \text{X (b) } p_y \pm i\tau p_x \rangle &= \sum_{\hat{\delta}} e^{-ia\vec{q} \cdot \hat{\delta}} t_x (\hat{y} \pm i\tau \hat{x}) \cdot \hat{\delta} \times \left[2 (\hat{x} \cdot \hat{\delta})^2 - 2i\tau (\hat{x}y \cdot \hat{\delta})^2 + i\tau - 1 \right] + \\ &+ \sum_{\hat{\delta}} e^{-ia\vec{q} \cdot \hat{\delta}} t_y (\hat{y} \pm i\tau \hat{x}) \cdot \hat{\delta}_\perp \times \left[2 (\hat{\delta} \cdot \hat{x}) (\hat{\delta}_\perp \cdot \hat{x}) - 2i\tau (\hat{\delta} \cdot \hat{x}y) (\hat{\delta}_\perp \cdot \hat{x}y) \right] \end{aligned} \quad (9)$$

where the unit vectors are defined as:

$$\begin{aligned} \hat{x} &= (1, 0) \\ \hat{y} &= (0, 1) \\ \hat{x}y &= \frac{1}{\sqrt{2}} (1, 1) \\ \text{and } \hat{\delta}_\perp &= (\delta_y, -\delta_x) \end{aligned} \quad (10)$$

and $\hat{\delta} = (\delta_x, \delta_y)$ are the three unit vectors connecting nearest-neighbors in the honeycomb lattice:

$$\hat{\delta} = \left\{ \hat{y}, \left(\frac{\sqrt{3}}{2}, -\frac{1}{2} \right), \left(-\frac{\sqrt{3}}{2}, -\frac{1}{2} \right) \right\} \quad (11)$$

This model for the case of MoS₂ leads to the electronic bands shown in Fig. 4.

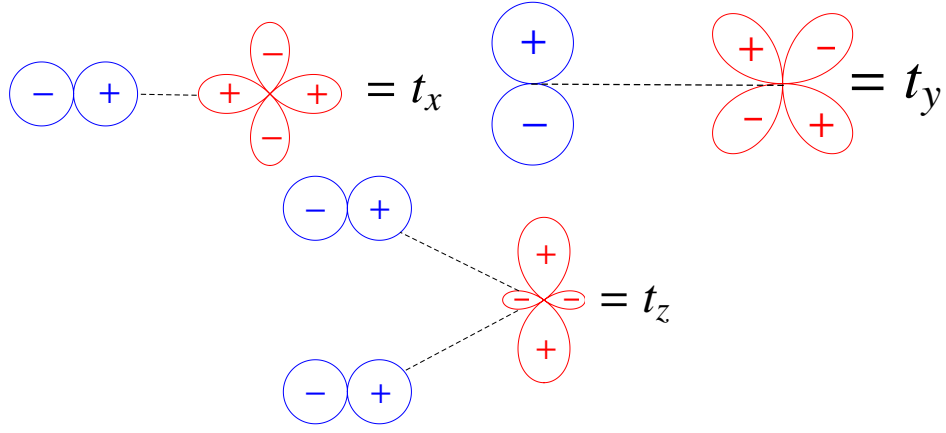


FIG. 3: Hopping integrals considered in the tight-binding model.

Tight-binding parameter	Value (eV)
Δ_0	-1.512
Δ_2	-3.025
Δ_p	-1.276
$V_{pd\sigma}$	-2.619
$V_{pd\pi}$	-1.396

TABLE II: Tight-binding parameters considered in the calculation. The values for MoS₂ are taken from Ref. 2.

$\mathbf{k} \cdot \mathbf{p}$ theory

At \mathbf{K}_τ points the Hamiltonian in first quantization reads as the matrix:

$$\begin{pmatrix} \Delta_0 & 0 & 3t_z & 0 \\ 0 & \Delta_2 & 0 & -3(t_x + t_y) \\ 3t_z & 0 & \Delta_p & 0 \\ 0 & -3(t_x + t_y) & 0 & \Delta_p \end{pmatrix} \quad (12)$$

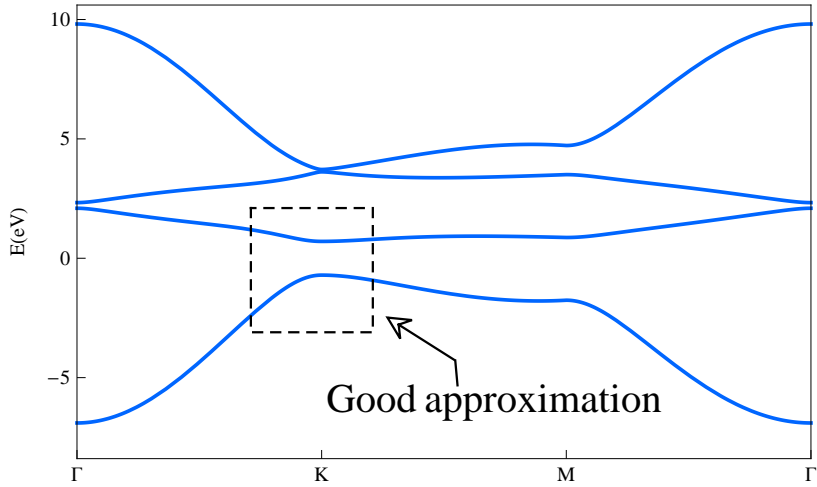


FIG. 4: Bands calculated within the tight-binding model described in the text. The model is only valid around \mathbf{K}_τ points (highlighted in the figure). We take the values summarized in Table II for MoS₂.

By diagonalizing this Hamiltonian we obtain the eigenvectors of the Bloch states maximally localized at $d_{3z^2-r^2}$ and $d_{x^2-y^2} + i\tau d_{xy}$ respectively, which define the conduction and band states respectively:

$$\begin{aligned} |\psi_c\rangle &= \frac{1}{\sqrt{1+|c|^2}} \begin{pmatrix} 1 \\ 0 \\ c \\ 0 \end{pmatrix} \\ |\psi_v\rangle &= \frac{1}{\sqrt{1+|v|^2}} \begin{pmatrix} 0 \\ 1 \\ 0 \\ v \end{pmatrix} \end{aligned} \quad (13)$$

where:

$$\begin{aligned} c &= -\frac{6t_z}{\sqrt{36t_z^2 + (\Delta_p - \Delta_0)^2 + \Delta_p - \Delta_0}} \\ v &= \frac{6(t_x + t_y)}{\sqrt{36(t_x + t_y)^2 + (\Delta_p - \Delta_2)^2 + \Delta_p - \Delta_2}} \end{aligned} \quad (14)$$

Then, the $\mathbf{k} \cdot \mathbf{p}$ Hamiltonian is just:

$$\mathcal{H}_{\mathbf{k} \cdot \mathbf{p}} = \begin{pmatrix} \langle \psi_c | \mathcal{H}_{TB} | \psi_c \rangle & \langle \psi_c | \mathcal{H}_{TB} | \psi_v \rangle \\ \langle \psi_v | \mathcal{H}_{TB} | \psi_c \rangle & \langle \psi_v | \mathcal{H}_{TB} | \psi_v \rangle \end{pmatrix} \quad (15)$$

If we write $\vec{q} = \mathbf{K}_\tau + \vec{k}$ and expand in powers of \vec{k} up to first order we get the Hamiltonian of Eq. (1) of the main text with:

$$\begin{aligned} \Delta &= \frac{1}{2} \left(\Delta_0 - \Delta_2 - \sqrt{36t_z^2 + (\Delta_0 - \Delta_p)^2} - \sqrt{36(t_x + t_y)^2 + (\Delta_2 - \Delta_p)^2} \right) = 1.41 \text{ eV} \\ t &= \frac{\sqrt{3} [c(t_x - t_y) + vt_z]}{2\sqrt{1+|c|^2}\sqrt{1+|v|^2}} = 1.19 \text{ eV} \end{aligned} \quad (16)$$

Coupling with strain

We repeat this calculation by considering the change in the hopping integrals $t_{x,y,z}$ due to the displacement of the atoms. For the hopping integral between atoms at sites α, β we have:

$$t_{\alpha\beta} \rightarrow t_{\alpha\beta} + \frac{\partial t_{\alpha\beta}}{\partial \mathbf{r}} (\mathbf{u}_\alpha - \mathbf{u}_\beta) \quad (17)$$

where $\mathbf{u}_{\alpha(\beta)}$ is the displacement of the atom at site α (β). For small displacements we can approximate:

$$\begin{aligned} \frac{\partial t_{\alpha\beta}}{\partial \mathbf{r}} &\approx \frac{\sqrt{3}}{a} t_{\alpha\beta} \beta_{\alpha\beta} \hat{\delta}_{\alpha\beta} \\ \mathbf{u}_\alpha - \mathbf{u}_\beta &\approx \frac{a}{\sqrt{3}} \hat{\delta}_{\alpha\beta} \cdot \vec{\partial} \mathbf{u} \end{aligned} \quad (18)$$

where $\beta_{\alpha\beta} \equiv -\partial \ln t_{\alpha\beta} / \partial \ln a$ is the Grüneisen parameter associated to $t_{\alpha\beta}$. Therefore, in the the previous matrix elements we have to consider now:

$$t_{x,y,z} \rightarrow t_{x,y,z} (1 + \beta_{x,y,z} \delta_i \delta_j u_{ij}) \quad (19)$$

where u_{ij} are the components of the strain tensor. By repeating the previous calculation at \mathbf{K}_τ we obtain the Hamiltonian of Eq. (2) of the main text with:

$$\begin{aligned} t\beta_0 &= \frac{3}{2} \left(\frac{c\beta_z t_z}{1+|c|^2} - \frac{v(\beta_x t_x + \beta_y t_y)}{1+|v|^2} \right) \\ t\beta_1 &= \frac{3}{2} \left(\frac{c\beta_z t_z}{1+|c|^2} + \frac{v(\beta_x t_x + \beta_y t_y)}{1+|v|^2} \right) \\ t\beta_2 &= \frac{3(c\beta_x t_x - c\beta_y t_y - v\beta_z t_z)}{4\sqrt{1+|c|^2}\sqrt{1+|v|^2}} \end{aligned} \quad (20)$$

Gaps induced by superlattice potentials and Haldane-Kane-Mele phase

We next provide the details of how a superlattice can be used to induce the subbands conduction and valence bands of a doped TMDCs. We approximate the bands of the homogeneous system by the two-band continuum-limit Hamiltonian introduced above, whose eigenvalues and eigenfunctions read:

$$\begin{aligned} \epsilon_{\vec{\mathbf{k}}} &= \pm \sqrt{\Delta^2 + (v|\vec{\mathbf{k}}|)^2} \\ |\vec{\mathbf{k}}\rangle &= \begin{pmatrix} \cos\left(\frac{\theta_{\mathbf{k}}}{2}\right) \\ \sin\left(\frac{\theta_{\mathbf{k}}}{2}\right) e^{i\phi_{\mathbf{k}}} \end{pmatrix} \end{aligned} \quad (21)$$

where $\theta_{\mathbf{k}} = \arctan[(v_F|\vec{\mathbf{k}}|)/\Delta]$ and $\phi_{\mathbf{k}} = \arctan(k_y/k_x)$.

A superlattice potential hybridizes states $|\vec{\mathbf{k}}\rangle$ and $|\vec{\mathbf{k}} + \vec{\mathbf{G}}\rangle$ where the vectors $\vec{\mathbf{G}}$ define the superlattice. We consider the six lowest vectors $\vec{\mathbf{G}}$, with $|\vec{\mathbf{G}}| = (4\pi)/(\sqrt{3}L)$, where $L = Na$ is the lattice constant of the $N \times N$ superlattice. We assume that $v|\vec{\mathbf{G}}| \ll \Delta$ and that the superlattice potential, $V_{\vec{\mathbf{G}}}$, is such that $V_{\vec{\mathbf{G}}} \ll (v|\vec{\mathbf{G}}|)^2/(2\Delta)$, so that perturbation theory in $V_{\vec{\mathbf{G}}}$ applies. We also assume that the lattice potential is sufficiently smooth, $|\vec{\mathbf{G}}| \ll |\vec{\mathbf{K}}_+ - \vec{\mathbf{K}}_-|$, where $\vec{\mathbf{K}}_{\pm}$ are the corners of the Brillouin Zone of the TMDC lattice, and neglect intervalley scattering.

Using first order perturbation theory, each set of three points at corners of the Brillouin Zone connected by superlattice reciprocal vectors leads to a 3×3 matrix:

$$\mathcal{H}_{\kappa, \kappa'} \equiv \begin{pmatrix} \epsilon_{\kappa, \kappa'} \pm \bar{v}k_x & V_{\kappa, \kappa'} & V_{\kappa, \kappa'}^* \\ V_{\kappa, \kappa'}^* & \epsilon_{\kappa, \kappa'} \pm \bar{v} \left(-\frac{k_x}{2} + \frac{\sqrt{3}k_y}{2} \right) & V_{\kappa, \kappa'} \\ V_{\kappa, \kappa'} & V_{\kappa, \kappa'}^* & \epsilon_{\kappa, \kappa'} \pm \bar{v} \left(-\frac{k_x}{2} - \frac{\sqrt{3}k_y}{2} \right) \end{pmatrix} \quad (22)$$

where $\epsilon_{\kappa, \kappa'} = \epsilon_0 = (v|\vec{\mathbf{K}}|)^2/(2\Delta)$, $\bar{v} \approx (v^2|\vec{\mathbf{K}}|)/\Delta$, and the two signs correspond to the κ and κ' points. For $V_{\kappa, \kappa'} = |V_{\kappa, \kappa'}| e^{i\phi_{\kappa, \kappa'}}$, the the energies and eigenfunctions at the κ and κ' points, in the basis used to write eq.(22) are:

$$\begin{aligned} \epsilon_a &= \epsilon_0 + 2|V_{\kappa, \kappa'}| \cos(\phi_{\kappa, \kappa'}) & |a\rangle &= \frac{1}{\sqrt{3}} (|1\rangle + |2\rangle + |3\rangle) \\ \epsilon_b &= \epsilon_0 + 2|V_{\kappa, \kappa'}| \cos\left(\frac{2\pi}{3} + \phi_{\kappa, \kappa'}\right) & |b\rangle &= \frac{1}{\sqrt{3}} (|1\rangle + e^{2\pi i/3} |2\rangle + e^{-2\pi i/3} |3\rangle) \\ \epsilon_c &= \epsilon_0 + 2|V_{\kappa, \kappa'}| \cos\left(\frac{4\pi}{3} + \phi_{\kappa, \kappa'}\right) & |c\rangle &= \frac{1}{\sqrt{3}} (|1\rangle + e^{-2\pi i/3} |2\rangle + e^{2\pi i/3} |3\rangle) \end{aligned} \quad (23)$$

In the case of $\phi_{\kappa, \kappa'} = 0, \pi$, then $V_{\kappa, \kappa'}$ real, an expansion in powers of $|\vec{\mathbf{k}}|$ shows that states $|b\rangle$ and $|c\rangle$ define an effective 2×2 Dirac Hamiltonian with velocity $\bar{v}/2$. For $\phi_{\kappa, \kappa'} = 0$ this Dirac point gives the lowest edge of the highest valence subband, and for $\phi_{\kappa, \kappa'} = \pi$ the upper edge of the lowest conduction band. The degeneracy of these Dirac points is lifted for complex values of $V_{\kappa, \kappa'}$. The problem is equivalent to a gapped Dirac equation with gap $\Delta_{\kappa, \kappa'} = 2\sqrt{3}|V_{\kappa, \kappa'}| \sin(\phi_{\kappa, \kappa'})$. If $\phi_{\kappa'}$ and ϕ_{κ} have different signs, the two gaps also have opposite signs, leading to a lowest subband with a Chern number equal to one. This is a realization of Haldane's model [3].

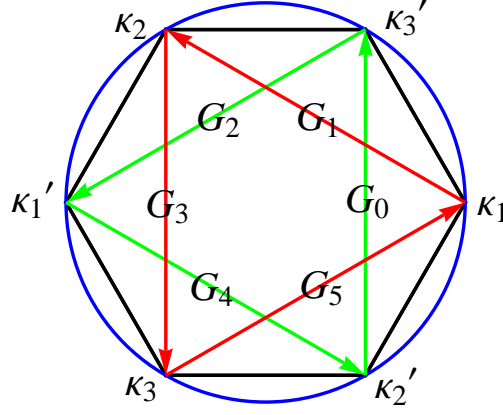


FIG. 5: (Color online). Sketch of the effect of the Brillouin Zone in a superlattice, and states mixed by the superlattice potential.

The superlattice potential is a 2×2 matrix in the space span by conduction and valence band states, and can be divided into scalar, mass and vector components, which, in turn, can be even or odd under spatial inversion. Following Ref. 4 we define the functions:

$$\begin{aligned} f_1(\mathbf{r}) &= \sum_{m=0\dots5} e^{i\mathbf{G}_m \cdot \mathbf{r}} \\ f_2(\mathbf{r}) &= i \sum_{m=0\dots5} (-1)^m e^{i\mathbf{G}_m \cdot \mathbf{r}} \end{aligned} \quad (24)$$

Then, we can construct the inversion-symmetric superlattice potentials as:

$$\begin{aligned} V_s &= v |\mathbf{G}| \Delta_s f_1(\mathbf{r}) \\ V_m &= v |\mathbf{G}| \Delta_m f_1(\mathbf{r}) \sigma_z \\ V_g &= v \Delta_g (\sigma_x, \tau_z \sigma_y) \cdot (\hat{z} \times \nabla) f_2(\mathbf{r}) \end{aligned} \quad (25)$$

The coefficients $\Delta_{s,m,g}$ in these expressions are dimensionless phenomenological constants with the energy scale set by $v |\mathbf{G}| = \frac{4\pi t}{\sqrt{3}N}$.

The scalar potential has matrix elements:

$$\langle \mathbf{k} + \mathbf{G}_m | V_s(\mathbf{G}_m) | \mathbf{k} \rangle = v |\mathbf{G}| \Delta_s \left[\cos\left(\frac{\theta_{\mathbf{k}+\mathbf{G}_m}}{2}\right) \cos\left(\frac{\theta_{\mathbf{k}}}{2}\right) + \sin\left(\frac{\theta_{\mathbf{k}+\mathbf{G}_m}}{2}\right) \sin\left(\frac{\theta_{\mathbf{k}}}{2}\right) e^{i(\phi_{\mathbf{k}} - \phi_{\mathbf{k}+\mathbf{G}_m})} \right] \quad (26)$$

Equivalently for the mass potential:

$$\langle \mathbf{k} + \mathbf{G}_m | V_m(\mathbf{G}_m) | \mathbf{k} \rangle = v |\mathbf{G}| \Delta_m \left[\cos\left(\frac{\theta_{\mathbf{k}+\mathbf{G}_m}}{2}\right) \cos\left(\frac{\theta_{\mathbf{k}}}{2}\right) - \sin\left(\frac{\theta_{\mathbf{k}+\mathbf{G}_m}}{2}\right) \sin\left(\frac{\theta_{\mathbf{k}}}{2}\right) e^{i(\phi_{\mathbf{k}} - \phi_{\mathbf{k}+\mathbf{G}_m})} \right] \quad (27)$$

The edges of the first subband are determined by the shifts in the energies of the corners of the superlattice Brillouin Zone. We assume that $|\mathbf{k}| = |\mathbf{k} + \mathbf{G}_m| = \kappa = (4\pi)/(3Na)$. Then:

$$\langle \mathbf{k} + \mathbf{G}_m | V_{s,m}(\mathbf{G}_m) | \mathbf{k} \rangle \approx v |\mathbf{G}| \Delta_{s,m} \left[1 - \frac{v^2 \kappa^2}{4\Delta^2} \left(1 \mp e^{i(\phi_{\mathbf{k}} - \phi_{\mathbf{k}+\mathbf{G}_m})} \right) \right] \quad (28)$$

For the gauge potential we have:

$$\begin{aligned} \langle \mathbf{k} + \mathbf{G}_m | V_g(\mathbf{G}_m) | \mathbf{k} \rangle &= i (-1)^m v |\mathbf{G}| \Delta_g \left[\cos\left(\frac{\theta_{\mathbf{k}+\mathbf{G}_m}}{2}\right) \sin\left(\frac{\theta_{\mathbf{k}}}{2}\right) e^{i(\phi_{\mathbf{k}} - \phi_{\mathbf{G}_m})} - \sin\left(\frac{\theta_{\mathbf{k}+\mathbf{G}_m}}{2}\right) \cos\left(\frac{\theta_{\mathbf{k}}}{2}\right) e^{i(\phi_{\mathbf{G}_m} - \phi_{\mathbf{k}+\mathbf{G}_m})} \right] \\ &\approx (-1)^m \frac{v\kappa}{\Delta} v |\mathbf{G}| \Delta_g e^{i\frac{\phi_{\mathbf{k}} - \phi_{\mathbf{k}+\mathbf{G}_m}}{2}} \cos\left(\frac{m\pi}{3} - \frac{\phi_{\mathbf{k}} + \phi_{\mathbf{k}+\mathbf{G}_m}}{2}\right) \end{aligned} \quad (29)$$

The same can be done with the inversion-asymmetric superlattice potentials, defined as:

$$\begin{aligned}\tilde{V}_s &= v |\mathbf{G}| \tilde{\Delta}_s f_2(\mathbf{r}) \\ \tilde{V}_m &= v |\mathbf{G}| \tilde{\Delta}_m f_2(\mathbf{r}) \sigma_z \\ \tilde{V}_g &= v \tilde{\Delta}_g (\sigma_x, \tau_z \sigma_y) \cdot (\hat{z} \times \nabla) f_1(\mathbf{r})\end{aligned}\tag{30}$$

By repeating the same calculation we obtain:

$$\begin{aligned}\langle \mathbf{k} + \mathbf{G}_m | \tilde{V}_{s,m}(\mathbf{G}_m) | \mathbf{k} \rangle &\approx i (-1)^m v |\mathbf{G}| \tilde{\Delta}_{s,m} \left[1 - \frac{v^2 \kappa^2}{4 \Delta^2} \left(1 \mp e^{i(\phi_{\mathbf{k}} - \phi_{\mathbf{k} + \mathbf{G}_m})} \right) \right] \\ \langle \mathbf{k} + \mathbf{G}_m | \tilde{V}_g(\mathbf{G}_m) | \mathbf{k} \rangle &\approx -i \frac{v \kappa}{\Delta} v |\mathbf{G}| \tilde{\Delta}_g e^{i \frac{\phi_{\mathbf{k}} - \phi_{\mathbf{k} + \mathbf{G}_m}}{2}} \cos \left(\frac{m\pi}{3} - \frac{\phi_{\mathbf{k}} + \phi_{\mathbf{k} + \mathbf{G}_m}}{2} \right)\end{aligned}\tag{31}$$

From this analysis it is clear that inversion-asymmetric potentials are needed in order to induce a topological subband structure. To the leading order in $v\kappa/\Delta$, considering scalar potentials only, we have:

$$\begin{aligned}V_\kappa &= \langle \kappa_1 = \kappa_2 + \mathbf{G}_4 | V_s(\mathbf{G}_4) + \tilde{V}_s(\mathbf{G}_4) | \kappa_2 \rangle = v |\mathbf{G}| \left(\Delta_s + i \tilde{\Delta}_s \right) \\ V_{\kappa'} &= \langle \kappa'_1 = \kappa'_2 + \mathbf{G}_1 | V_s(\mathbf{G}_1) + \tilde{V}_s(\mathbf{G}_1) | \kappa'_2 \rangle = v |\mathbf{G}| \left(\Delta_s - i \tilde{\Delta}_s \right)\end{aligned}\tag{32}$$

So $V_{\kappa, \kappa'} = v |\mathbf{G}| \sqrt{\Delta_s^2 + \tilde{\Delta}_s^2} \times e^{\pm i \arctan(\frac{\tilde{\Delta}_s}{\Delta_s})}$. Hence, the gap is $\Delta_{\kappa, \kappa'} = \pm 2\sqrt{3}v |\mathbf{G}| \tilde{\Delta}_s$. Either the lowest conduction or valence subbands derived from the bands at a given spin polarized valley in the band structure of the TMDC have a Chern number equal to one. This Chern number is compensated by the opposite value from the other valley due to time-reversal symmetry. Therefore, this system is effectively a realization of the Kane-Mele model [5].

-
- [1] J. C. Slater and G. F. Koster, Phys. Rev. **94**, 1498 (1954).
 - [2] E. Cappelluti, R. Roldán, J.A. Silva-Guillén, P. Ordejón, F. Guinea, Phys. Rev. B **88**, 075409 (2013).
 - [3] F. D. M. Haldane, Phys. Rev. Lett. **61**, 2015 (1988).
 - [4] J. R. Wallbank, A. A. Patel, M. Mucha-Kruczynski, A. K. Geim, and V. I. Fal'ko, Phys. Rev. B **87**, 245408 (2013).
 - [5] C. L. Kane and E. J. Mele, Phys. Rev. Lett. **95**, 226801, *ibid* 146802 (2005).
-